



Joint Geophysical Investigation of Uteh Gully Erosion and Landslides Using Electrical Resistivity Tomography and Multichannel Analysis of Surface Waves

Egbo, D.O.¹ and Airen, O.J.²

^{1,2} Department of Physics, Faculty of Physical Sciences, University of Benin, Benin City 302001, Nigeria.

Corresponding author E-mail: okeegbo@gmail.com

Article Info

Keywords:

Gully, Shear Modulus, Dry Sand and Res2dinv

Received 08 February 2023

Revised 02 March 2023

Accepted 02 March 2023

Available online 15 March 2023

<https://doi.org/10.5281/zenodo.7737981>

ISSN-2682-5821/© 2023 NIPES Pub. All rights reserved.

Abstract

Joint investigation of gully erosion and landslides was carried out by employing Electrical Resistivity Tomography (ERT) and Multichannel Analysis of Surface Waves (MASW) methods of geophysical investigation. Data were acquired using PASI 16GL model resistivity meter and a 24-channel ABEM Terralock MATK-6 seismograph for ERT and MASW respectively along two traverses each. Data acquired for ERT and MASW were processed with Res2dinv and SeisImager2D refraction software developed by Geometric Earth Science Ltd respectively and a 2-D resistivity image and 2-D shear wave (Vs) and P-wave (Vp) velocities of the subsurface were generated. 2-D resistivity subsurface imaging reveals presence of topsoil, clay, sand and coarse sand. The shear wave velocity and elastic parameters reveals soil ranging from soft to medium-stiff clays/dry sand/wet sand and medium-stiff to stiff saturated clays/dry sand/wet sand. This shows the susceptibility of the area to gully erosion due to incompetent soil structures.

1.0. Introduction

A major environmental problem ravaging southern Nigeria is the high torrential rainfall experienced in the region which creates a thriving environment for catastrophic soil erosion [1]. The devastating impact of gully erosion on lives, physical and socio-economic activities cannot be overemphasized. According to the World Bank Country report on Nigeria in 2009, gully erosion is reported to be one of the top five hazards posing a threat to the environment [2]. Generally, soil loss and gully erosion are particularly driven by lithology, climate change, land use and land cover change amongst many other factors [3]. According to field observations and geotechnical evaluation of gully erosion in Iguosa Benin City Edo State, slope steepness, weakly developed structure, unconsolidated soil structure, less cohesion and high permeability amongst other factors contributes to landslide and gully erosion in the study area [4]. Properties worth millions of Naira has been lost to gully erosion and so many under threat. About 10 houses have been lost in a single event of gully erosion in Auchi area of Edo State. It was also gathered recently that over 450

buildings are lost in Edo State of Nigeria as a result of erosion (NTA News, Sunday 6th July 2013)
[5]. Farming which is identified as a source of livelihood is not left out. The effect of gully is a

threat to food security in the country as a result of landmass lost to gullies. The economic damage brought by gullies, mainly in Nigeria's southeast, could be up to \$100 million every year, with an agricultural yield losses of 30 to 90% in some areas [6]. Several scholars have studied factors and mechanisms that affects gully erosion and landslides adopting various methods. Geophysical methods are indispensable for the recognition and interpretation of structures within the subsurface as they respond to the physical properties of the subsurface media (e.g., rocks, sediments, water, voids, etc.) and can be applied successfully resulting that a region differs sufficiently from another in some physical property. One of the many direct ways in which geophysical investigation aids the general economy is in the delineation of subsurface lithology or rock types [7]. Joint geophysical methods have played significant roles in exploring for natural resources, environmental issues and geotechnical investigations. An investigation of the internal structures of landslides in South Eastern Nigeria using Electrical Resistivity Tomography (ERT) revealed that the area consists of clayey and sandstone formation with mostly low resistivity values indicative of shale layers and groundwater zones [8]. The Electrical Resistivity Tomography (ERT) and Multichannel Analysis of Surface Waves was integrated in mapping the subsurface of a wetland area of Lagos Nigeria. Joint interpretation reveals that the site of investigation is characterized with weak/incompetent materials not suitable for hosting foundation of massive engineering structures [9]. Landslides have been characterized using MASW and ERT methods successfully [10]. A 2DNear-Surface Litho-Structural Geophysical Investigation at the Vicinities of Two Gully-Erosion/Landslide Sites in South Eastern Nigeria involving seismic refraction tomography (SRT) and electrical resistivity tomography (ERT) was carried out. The analysis and interpretation of the joint approach revealed that the interpreted lithology are causative to the relatively active and severely active gully sites in the area under investigation [11]. The aim of this studies is to delineate the stiffness and lithology of the subsurface in the study location using Electrical Resistivity Tomography (MASW) and Multichannel Analysis of Surface Waves (MASW).

Table 1: Site Classification of Shear Wave Velocity by NEHRP [12]

NEHRP Site Classification	Average Shear Wave Velocity (Vs) (m/s)
Special Study	Less than 100
Soft	100 to 200
Medium Stiff	200 to 375
Stiff	375 to 700
Rock	Greater than 700

2.0 Methodology

2.1. Local geologic settings

The survey area is located within longitudes 005° 38' 52.28" E to 005° 38' 57.47" E, latitudes 06° 23' 13.12" N to 06° 23' 14.71" N and elevation of 31 to 36 m at Uteh gully erosion site situated in Ovia North East Local Government Area. The area also occupies the Southern part of Edo State which is underlain by sedimentary formation whose geology falls under Benin Formation of the Niger Delta Basin. The formation consists of top reddish clayey sand capping highly porous fresh water bearing loose pebbly sands, sand and sandstone with local thin clays and shale inter-beds which are considered to be of braided stream origin. It is characterized by deposits laid during tertiary and cretaceous periods and is underlain by sedimentary rocks of Paleocene to recent age.

The Benin Formation locally covered with Quaternary drift (loose brownish sand) varies in thickness but attains a maximum thickness of 6000ft (approx. 1970m) near the sea shore. The sedimentary rock contains about 90% of sand stone and shale intercalations [13]. Edo State is situated in South-western part of Nigeria. It is an important sedimentary basin in Nigeria due to her closeness to the oil fields within the Niger-Delta region.

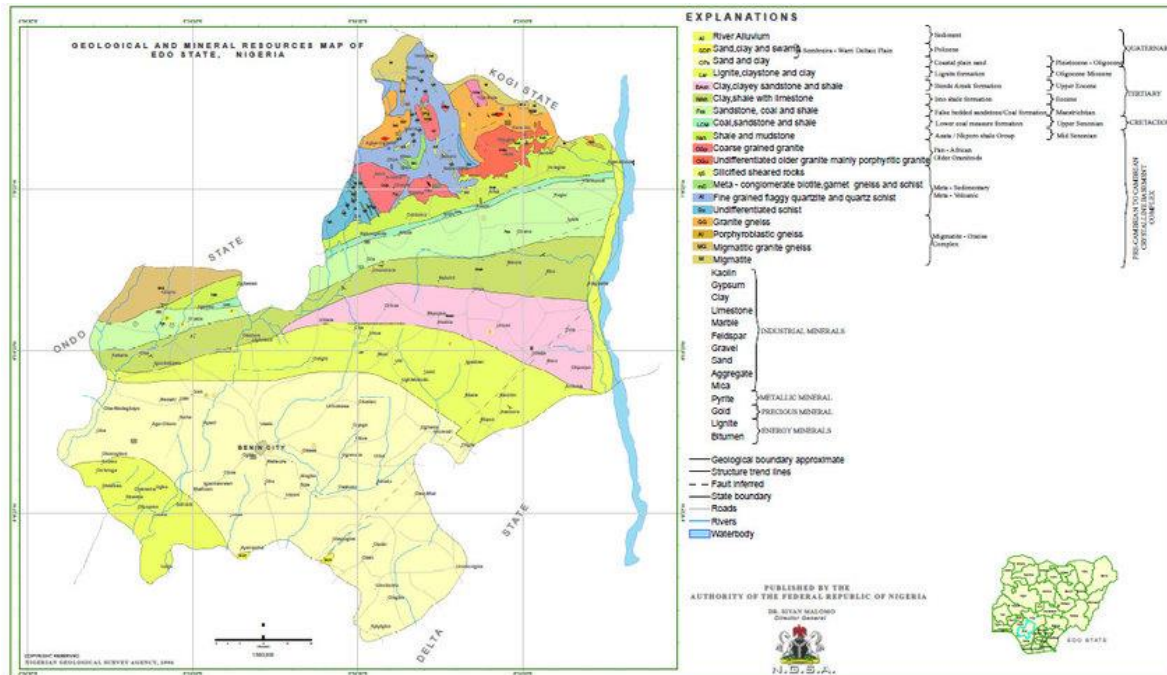


Figure 1: Map of Edo State showing the study area (Ministry of Environment, Benin City)

2.2. Theory of Electrical Resistivity Tomography

Electrical Resistivity methods have been successful in engineering and environmental geological investigations, as important information on geological structure, lithology and subsurface water resources can be revealed without the large cost of an extensive drilling activities. Electrical methods utilize direct currents or low frequency alternating currents to investigate differences in the electrical properties of materials in the subsurface [14].

Fundamentally, the electrical resistivity surveys are based on the Ohm's law propounded by the German physicist Georg Simon Ohm in 1827, which governs the current flow in the ground. This establishes a relationship between the electric current I in a conducting wire, and the potential difference V across it. Therefore, Ohm's can be represented by the linear equation.

$$V = IR \quad (1)$$

Where R is the resistance of the conducting medium.

Let us consider a material of length L , with current I flowing through the material as shown in the Figure 2.1. The resistance offered by the material is proportional to the length and inversely proportional to the cross-sectional areal A of the material given by the equation:

$$R = \rho \frac{L}{A} \quad (2)$$

Where ρ is the resistivity of the conductor measured in ohm-m (Ωm) representing the constant of proportionality. The inverse of ρ is the conductivity σ (Siemens per meter) of the material [15].

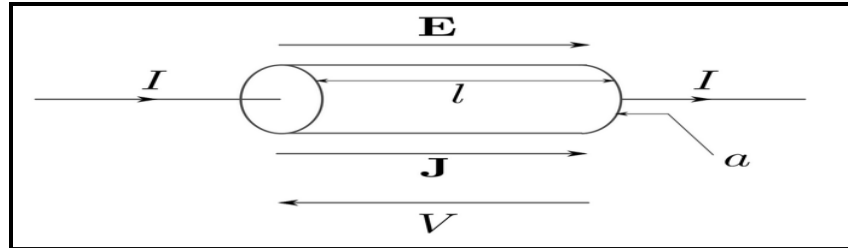


Figure 2: Parameters used in the definition of Ohms Law [16]

From the Figure 2 above, we can deduce the Electric Field E and current density J which are expressed in equations below as;

$$E = \frac{V}{L} \quad (3)$$

$$J = \frac{I}{A} \quad (4)$$

By substituting equation (2) into equation (1), and rearranging the terms, we obtain

$$\frac{V}{L} = \rho \frac{I}{A} \quad (5)$$

Substituting equations (3) and (4) into equation (5), we have

$$E = \rho J \quad (6)$$

Since $\rho = 1/\sigma$ Ohm's law can be written in vector form as:

$$J = \sigma E \quad (7)$$

where J is the current density, E is the electric field intensity, and σ is the electrical conductivity with unit of siemens/m or mho/m. the reciprocal of resistivity ρ ($\sigma = 1/\rho$).

In practice the electric potential V is measured. The relationship between V and E is given by:

$$E = -\text{grad}V \quad (8)$$

Combining above equations (1) and (2) we get:

$$J = -\sigma \text{grad}V \quad (9)$$

Let us consider the case of a homogeneous isotropic subsurface and a single point current source on the ground surface. In this case, the current flows radially away from the source.

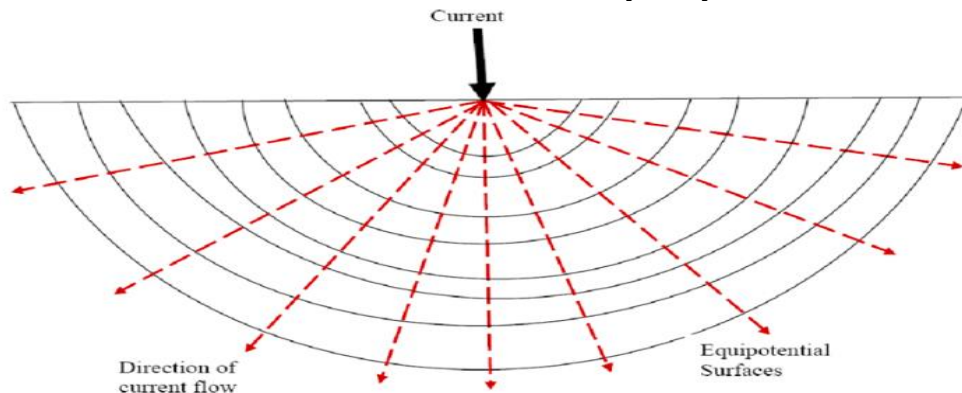


Fig. 3: Homogeneous isotropic subsurface

The equipotential surfaces develop into a hemispherical shape, with the current flow perpendicular to the equipotential surface. At some distance r from the current source, the hemispherical shell has surface area $2\pi r^2$ and therefore the current density J is:

$$J = I/2\pi r^2 \quad (10)$$

Since $\rho = 1/\sigma$ and using $J = I/2\pi r^2$ then equation $J = -\sigma \text{ grad } V$ can be written as

$$\begin{aligned} \frac{I}{2\pi r^2} &= -\frac{1}{\rho} \frac{\partial V}{\partial r} \\ -\frac{\partial V}{\partial r} &= \frac{\rho I}{2\pi r^2} \end{aligned} \quad (11)$$

By integrating the above equation, we obtain the potential V at a distance r from the current source as:

$$\begin{aligned} V &= \int_r^\infty (\rho I/2\pi r^2) dr = \rho I/2\pi r \\ V &= \frac{\rho I}{2\pi r} \end{aligned} \quad (12)$$

Where,

U = potential, in Volts (V), ρ = resistivity of the medium, r = distance from the electrode. Equation 6 is the fundamental relationship for electrical survey carried out at the surface of a uniform isotropic earth. Data from resistivity surveys are customarily presented and interpreted in the form of values of apparent resistivity ρ_a .

Apparent resistivity is defined as the resistivity of an electrically homogeneous and isotropic half-space that would yield the measured relationship between the applied current and the potential difference for a particular arrangement and spacing of electrodes. An equation giving the apparent resistivity in terms of applied current, distribution of potential, and arrangement of electrodes can be arrived at through an examination of the potential distribution due to a single current electrode. The effect of an electrode pair (or any other combination) can be found by superposition.

For an electrode pair with current $+I$ at electrode A, and $-I$ at electrode B (Figure 4), the potential at a point is given by the algebraic sum of the individual contributions:

$$V = \frac{\rho I}{2\pi r_A} - \frac{\rho I}{2\pi r_B} = \frac{\rho I}{2\pi} \left[\frac{1}{r_A} - \frac{1}{r_B} \right] \quad (13)$$

Where, r_A and r_B = distances from the point to electrodes A and B

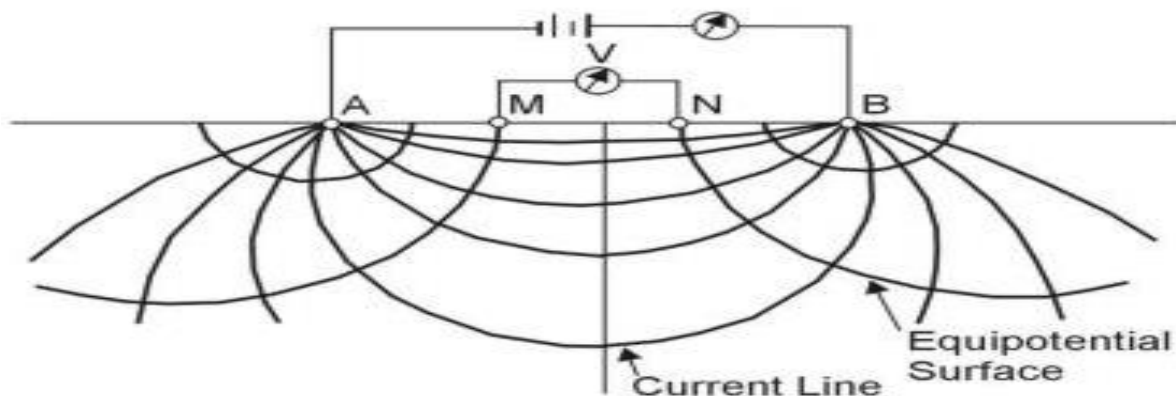


Figure 4: Equipotential and current lines for a pair of current electrodes A and B on a homogeneous half-space [15]

In addition to current electrodes A and B, Figure 4 shows a pair of electrodes M and N, which carry no current, but between which the potential difference V may be measured. Following the previous equation, the potential difference V may be written as:

$$V = U_M - U_N = \frac{\rho I}{2\pi} \left[\frac{1}{AM} - \frac{1}{BM} + \frac{1}{BN} - \frac{1}{AN} \right] \quad (14)$$

Where;

U_M and U_N = potentials at M and N; AM = distance between electrodes A and M,
BM = distance between electrodes B and M; BN = distance between electrodes B and N,
AN = distance between electrodes A and N,

The quantity, $1/K$ allows the rewriting the equation as:

$$V = \rho \frac{I}{K} \quad (15)$$

Equation 4 can be solved for ρ to obtain:

$$\rho = K \frac{V}{I} \quad (16)$$

From Ohm's law, equation 2.16 can be written as;

$$\rho = KR \quad (17)$$

Where K = geometrical coefficient that depends on the arrangement of the four electrodes A, B, M and N.

The value of apparent resistivity is a function of several variables; the electrode spacing, the geometry of the electrode array, and the true resistivity and other characteristics of subsurface material, such a layer thickness, angle of dip, anisotropic properties. The apparent resistivity, depending on the electrode configuration and on the geology, may be crude average of the true resistivity in the section, maybe larger or smaller than any of the true resistivity, or may be negative [15]. Figure 5 show a list of common arrays along with their geometric factor (K).

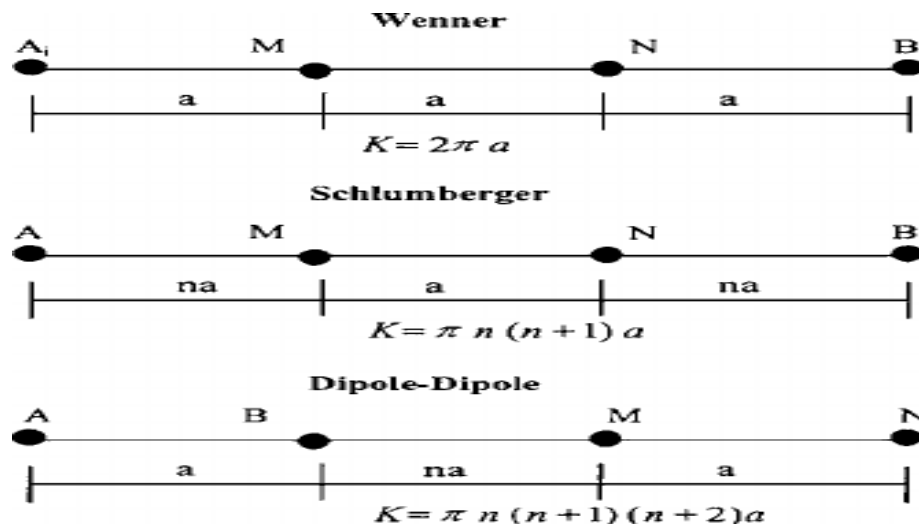


Figure 5: Common arrays used in resistivity surveys and their geometric factors [17]

The Wenner array electrode configuration was adopted for this studies with geometric factor $K=2\pi a$. Accordingly, Equation 17 becomes:

$$\rho_a = 2\pi aR \quad (18)$$

Electrical Resistivity Tomography (ERT) data was acquired using PASI 16GL model resistivity meter adopting Wenner electrode configuration. Electrodes were coupled with the ground using the hammer till good contact was made to the ground. The current and voltage electrodes were connected to the resistivity meter via the reels of electric cables using alligator clips so as to ensure firm and good connection. Current was supplied to the current electrodes by the resistivity meter and the corresponding values of the resistivity, voltage and current were read off on the PASI resistivity meter and recorded. The cables were checked after each ERT data was acquired.

Using this technique, data were acquired and the resistivity imaging were interpreted geologically using the standard resistivity values for rocks, minerals and sediments from available literatures and also using the knowledge of the local geology of the research area. Table 1 shows some earth materials and their respective resistivity.

Table 2: Typical values of some earth material [18]

MATERIAL	RESISTIVITY (ΩM)
Alluvium	10 to 800
Sand	60 to 1000
Clay	1 to 100
Groundwater (fresh)	10 to 100
Sandstone	$8 - 4 \times 10^3$
Shale	$20 - 2 \times 10^3$
Limestone	$50 - 4 \times 10^3$
Granite	5,000 to 1,000,000

2.3. Theory of Multichannel Analysis of Surface Waves

The measurement of shear wave velocity is necessary for analyzing variations in subsurface stiffness [19]. Small strain parameters of subsurface materials can be studied by evaluating change in stress. Multichannel analysis of surface waves (MASW) is a non-destructive seismic method which analyzes the dispersion properties of horizontal traveling Rayleigh surface waves [19]. The multichannel analysis of surface waves (MASW) method deals with surface waves in the lower frequencies of 1-30 Hz. Shear modulus is directly linked to a material's stiffness and is one of the most critical engineering parameters. Seismically, shear-wave velocity (VS) is its best indicator. Seismic theory is dependent on the idea that elastic waves travel at speeds which correlate with the physical properties the respective media [20]. Recognizing this requires an initial physical understanding of material elastic behavior and wave velocity.

The physics of MASW is based on the principle of surface wave propagation, dispersion and the relationship between the shear wave velocity structure of the subsurface and the properties of these surface waves. It utilizes the principle of wave physics to measure, analyze and map shallow subsurface structure. According to Hooke's law, the strain, experienced by an object is directly related to the imposed stress, σ , on that given object. When no permanent deformation is experienced, the elastic material property that directly correlates strain to stress is termed the elastic modulus, E [21].

$$\sigma = \epsilon E \quad (19)$$

Wave propagation is dependent on the ability to elastically deform particles within a given media. The propagation of different wave types is caused by the different forms of stress imposed (e.g. compressive stress, shearing stress). In different situations, the applicability of the small strain assumption has been questioned and other model relating to stress and strain have been applied to seismic analysis. However, the principle of Hooke's law remains one of the prominent models for elasticity in seismic theory [20].

The wave velocity, v , is directly related to the frequency of the wave, f , and the length of the wave, λ , as

$$v = \lambda f \quad (20)$$

The wavelength is the distance between two consecutive wave peaks or troughs. The frequency of a wave is the reciprocal of the wave period, T , which is the duration required to complete one wave oscillation.

$$f = \frac{1}{T} \quad (21)$$

In S-wave propagation, particles move perpendicular to the direction of wave movement. In a homogeneous environment, the velocity of a body can be expressed by the general equation provided below.

$$V = \sqrt{\left(\frac{\text{material elastic modulus}}{\text{material density, } \rho}\right)} \quad (22)$$

Measurements are carried out at the surface, using a swept-frequency source and at least two geophones. The swept-frequency source provides a known frequency for the velocity calculation. Received signals are used determine the phase difference for each frequency. Travel time is represented in Equation (23), where the frequency, f , is represented in hertz and the phase difference φ , is in radians.

$$t(f) = \left[\frac{\varphi(f)}{(2\pi f)} \right] \quad (23)$$

The wave velocity, can then be measured by relating the known distance between the receiver spread and travel time, as seen in Equation 24.

$$V = \left[\frac{d_2 - d_1}{t(f)} \right] \quad (24)$$

The velocity is then used to determine the wavelength of the respective Rayleigh wave, using the general wave relationship presented in Equation 24. Multiple measurements of phase velocity and wavelength are made by reconfiguring the receiver spread and/or varying the transmitted frequency. The relationship between phase velocity and wave length is then plotted to develop a surface wave dispersion curve. Through an inversion process, the dispersion curve can be transformed into a representative earth model relating shear wave velocity with depth [22].

MASW data were acquired using a 24-channel ABEM Terralock MATK-6 seismograph with geophones of frequency 14Hz and the geophone array was monitored to ensure all geophones were correctly connected and coupled with the ground. A hammer of weight 8 Kg was used as seismic source to generate seismic energy by impacting on a metal plate on the ground. Energy generated at each point were stacked to improve the definition of the record. The recording time and sampling intervals were set at 1 second and 0.5 millisecond respectively. After the initial setup, the system was ready for the first shot record. Recording sequence is started by initializing the recording software and arming the trigger system. When ready, the party responsible for swinging the hammer is signaled, and the hammer blow initiates the survey. The response from the triggering system notifies the seismograph that the survey has begun. Signals recorded through the designated recording time and at the designated time interval. After sounding is accepted, the setup is then moved for the next sounding. A total of 3 traverse were recorded during this survey.

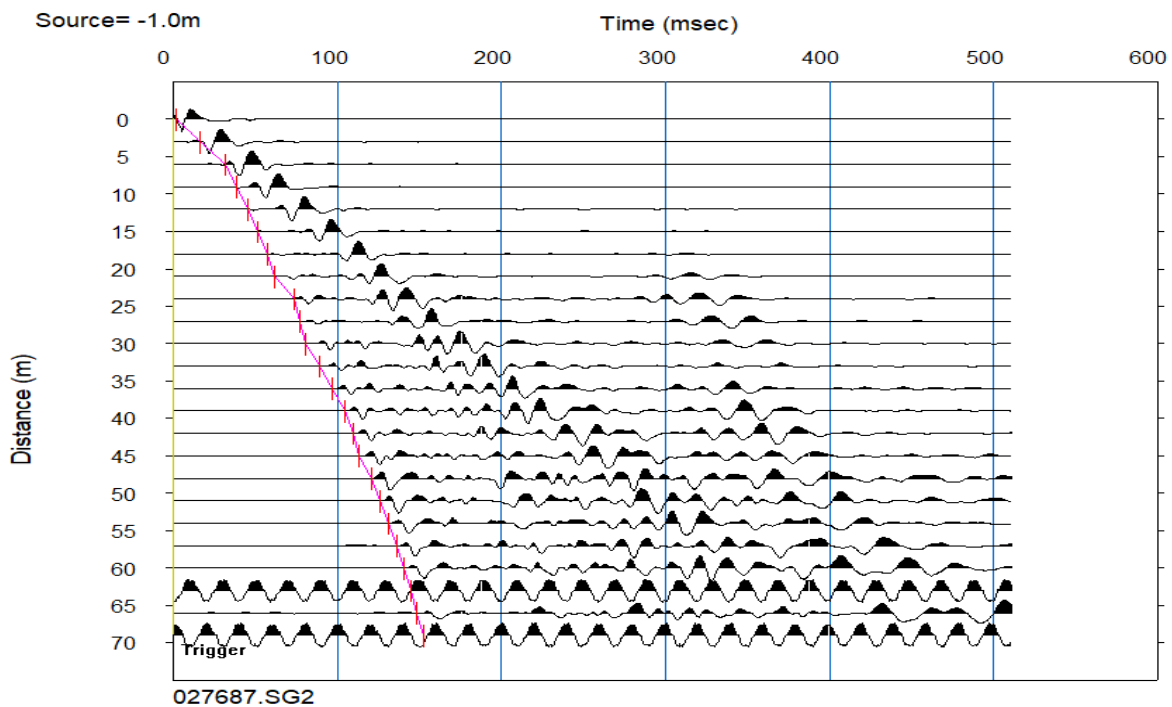


Figure 6: Visual Output of Acquired Unprocessed Record of MASW Shot

3.0. Results and Discussion

3.1. Electrical Resistivity Tomography (ERT)

Investigation of the gully in Uteh was carried out using PASI 16GL model resistivity meter to measure the resulting electrical potential V from current I injected into the subsurface. The apparent resistivity was computed using Equation 18. Data collected were processed with Res2dinv software and a 2D imaging of the subsurface was obtained which is the true subsurface resistivity. The subsurface resistivity is then used to deduce the geological characteristics of the surveyed depth range.

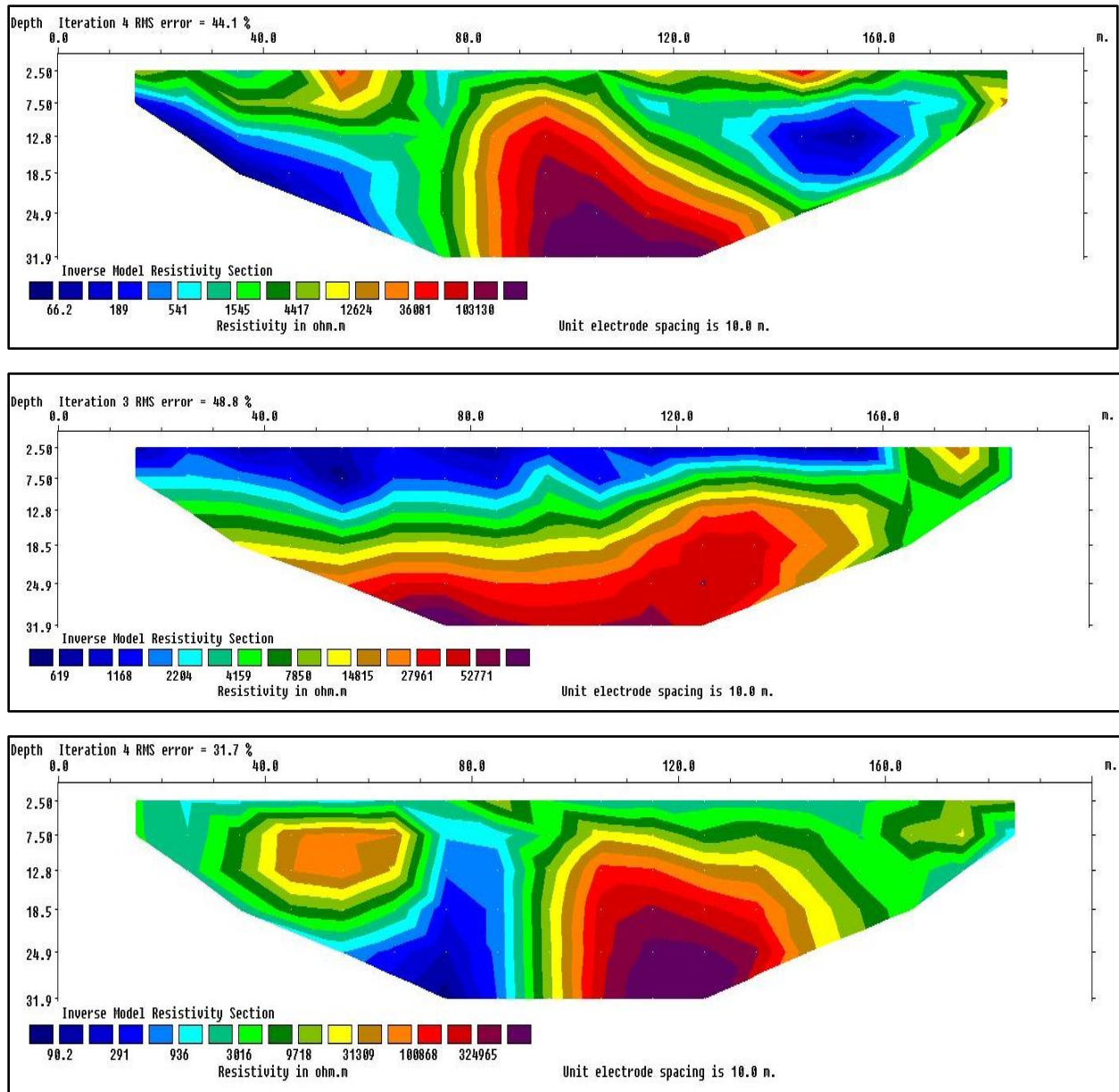


Figure 7: 2-D Electrical Resistivity Structure Along Traverse 1 – 3 (UTEH)

The inverted 2D resistivity structure along traverse 1 – 3 at Uteh erosion site is presented in Figure 7 revealing to distance and depth of 180 m and 31.9 m respectively. The resistivity value along these profiles ranges from about 66.2 ohm-m to more than 324965 ohm-m. Three resistivity zones are recognizable on these resistivity structures. The first geoelectric zone (blue colour zones) is characterized by resistivity values ranging from about 66.2 ohm-m to about 2204 ohm-m. The second geoelectric zone (green - yellow) is characterized by resistivity value falling between 1545 ohm-m to about 31309 ohm-m. The third resistivity zone (red – purple colour) is characterized by resistivity value ranging from 27961 ohm-m to far greater than 324965 ohm-m. This zone has the most resistive material along these profiles and as has a higher erodibility potential.

3.2. Multichannel Analysis of Surface Waves (MASW)

Joint investigation involving MASW was carried out and data were acquired using a 24-channel ABEM Terralock MATK-6 seismograph with geophones of frequency 14Hz. Shots recorded was processed using SeisImager2D refraction software developed by Geometric Earth Science Ltd. The first step of seismic refraction data processing is the accurate picking of the first breaks corresponding to the geophones in the profile using the Pickwin module, then the time-distance curve for the profile is generated based on the profile length, geophone spacing, shooting locations, and the first arrival times. The second step is to develop the dispersion curve which is considered one of the most critical steps for generating an accurate shear-wave velocity profile. This step starts by selecting the frequency domain which in this study ranges from 5 to 40Hz. Thirdly, the dispersion curve is edited as needed to eliminate noisy picks on the low and high-frequency ends of the curve. The final step is to set up the initial model of shear wave velocity with depth and set the suitable number of iterations for the data inversion to converge on the best fit of the initial model with the observed data and the final 2-D S-wave velocity profile is displayed. The root mean square errors (RMSE) of our final velocity-depth profiles are less than (5%). The iterative process continues until the predetermined error tolerance is achieved or the maximum number of iterations is performed. The elastic parameters were generated using the formula presented in the Table 3.

Table 3: Formula for generating elastic parameters [23].

S/N	ELASTIC PARAMETER	EQUATION
1	Bulk Modulus, K	$K = \rho(V_P^2 - \frac{4}{3}V_S^2)$
2	Poisson's Ratio, V	$V = \frac{V_P^2 - 2V_S^2}{2(V_P^2 - V_S^2)}$
3	Shear Modulus, μ	$\mu = \rho V_S^2$
4	Young's Modulus, E	$E = \frac{\rho V_S^2(3V_P^2 - 4V_S^2)}{V_P^2 - V_S^2}$

The results obtained from the six traverses in 2-D are presented in Figure 8.

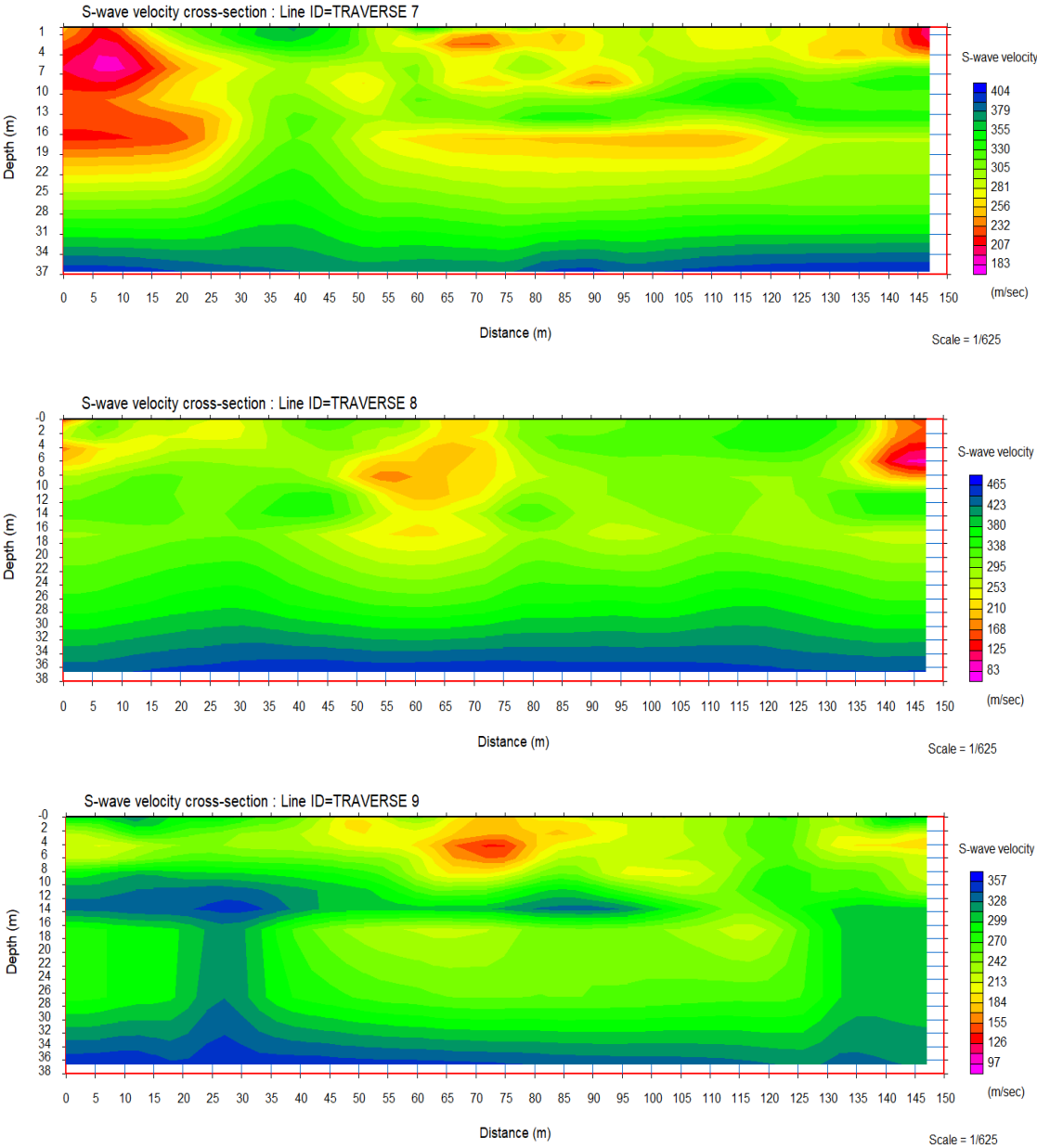


Figure 8: 2-D Shear Wave Velocity Model Along Traverse 1 – 3

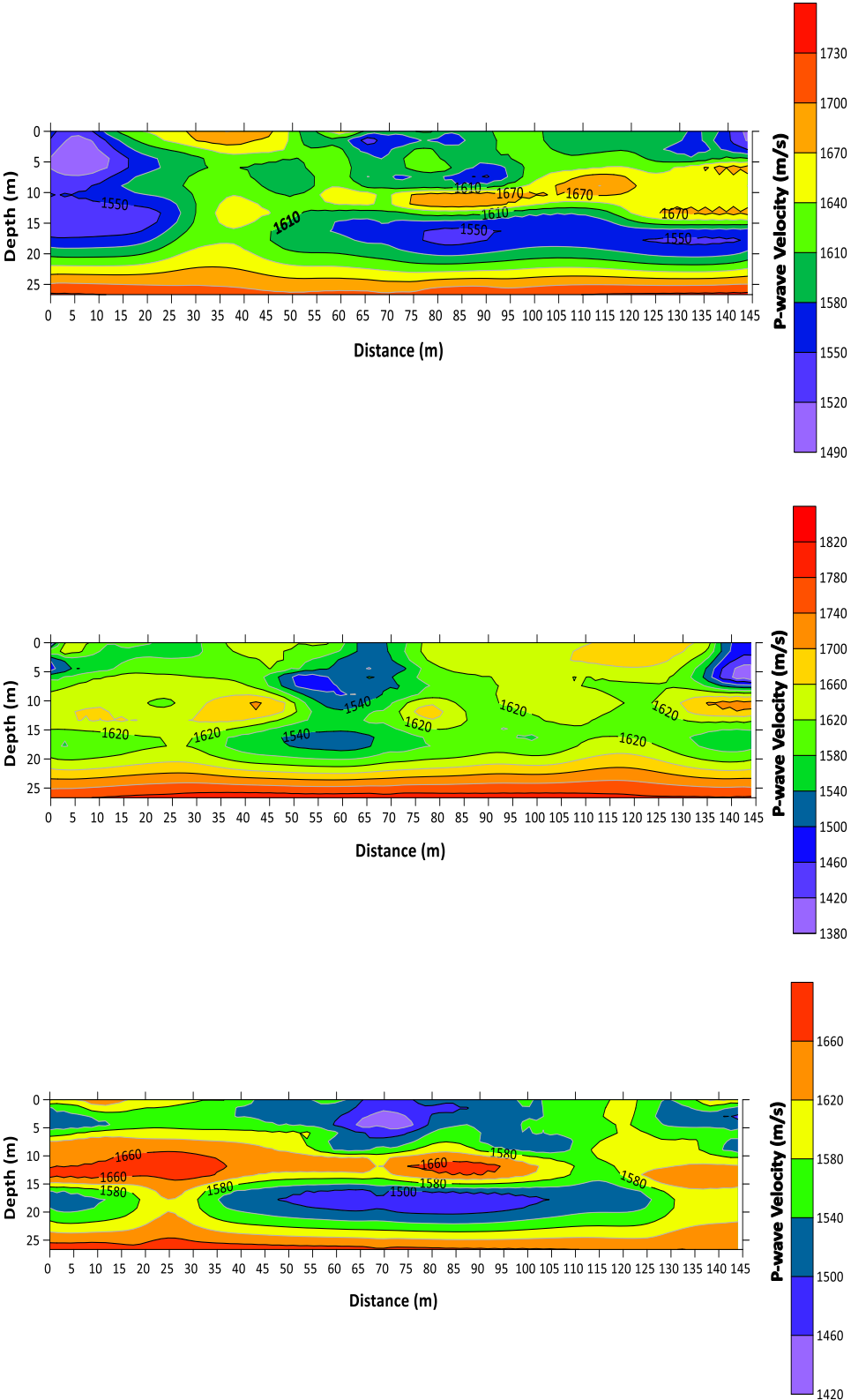


Figure 9: 2-D P-wave Velocity Along Traverse 1 – 3

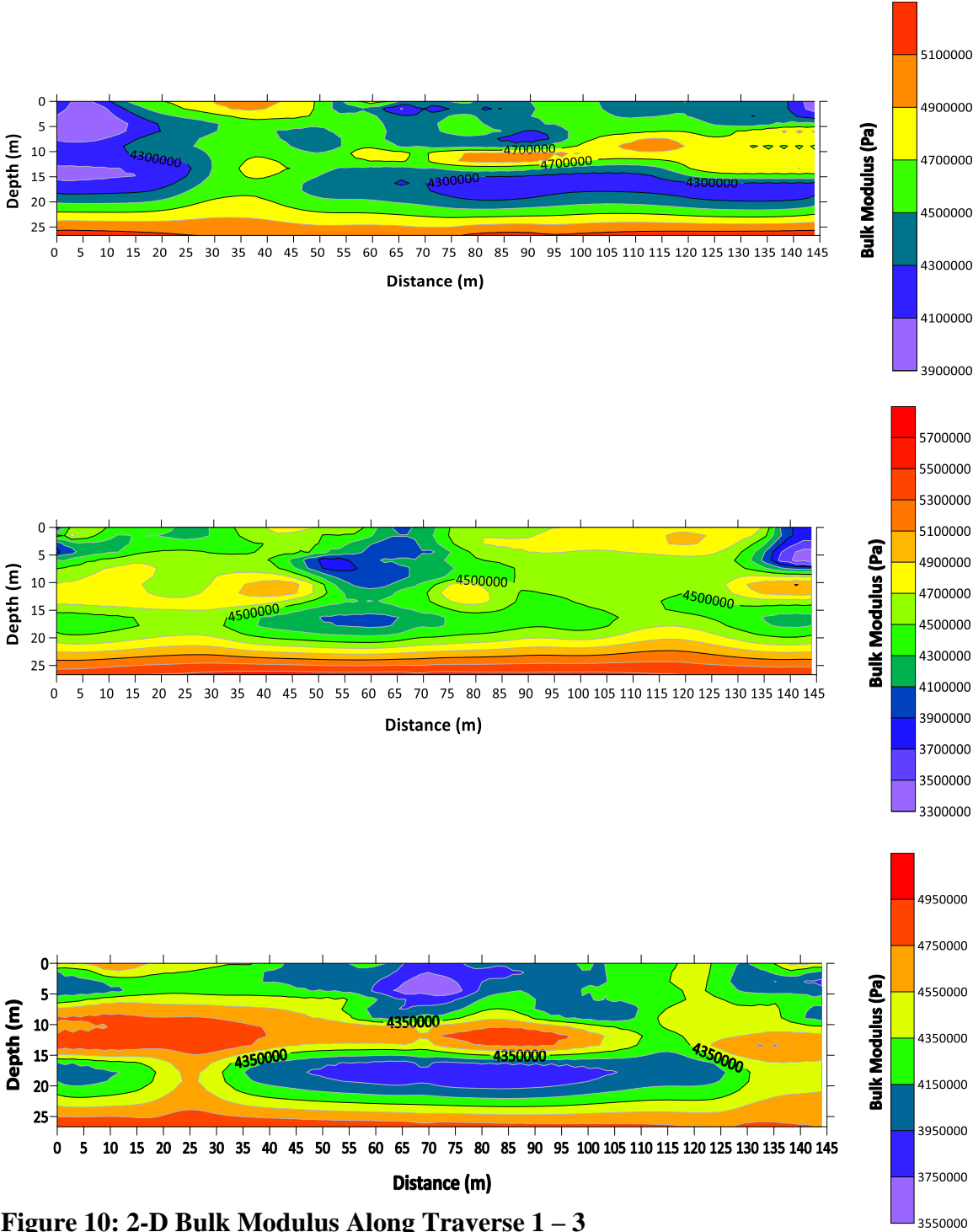


Figure 10: 2-D Bulk Modulus Along Traverse 1 – 3

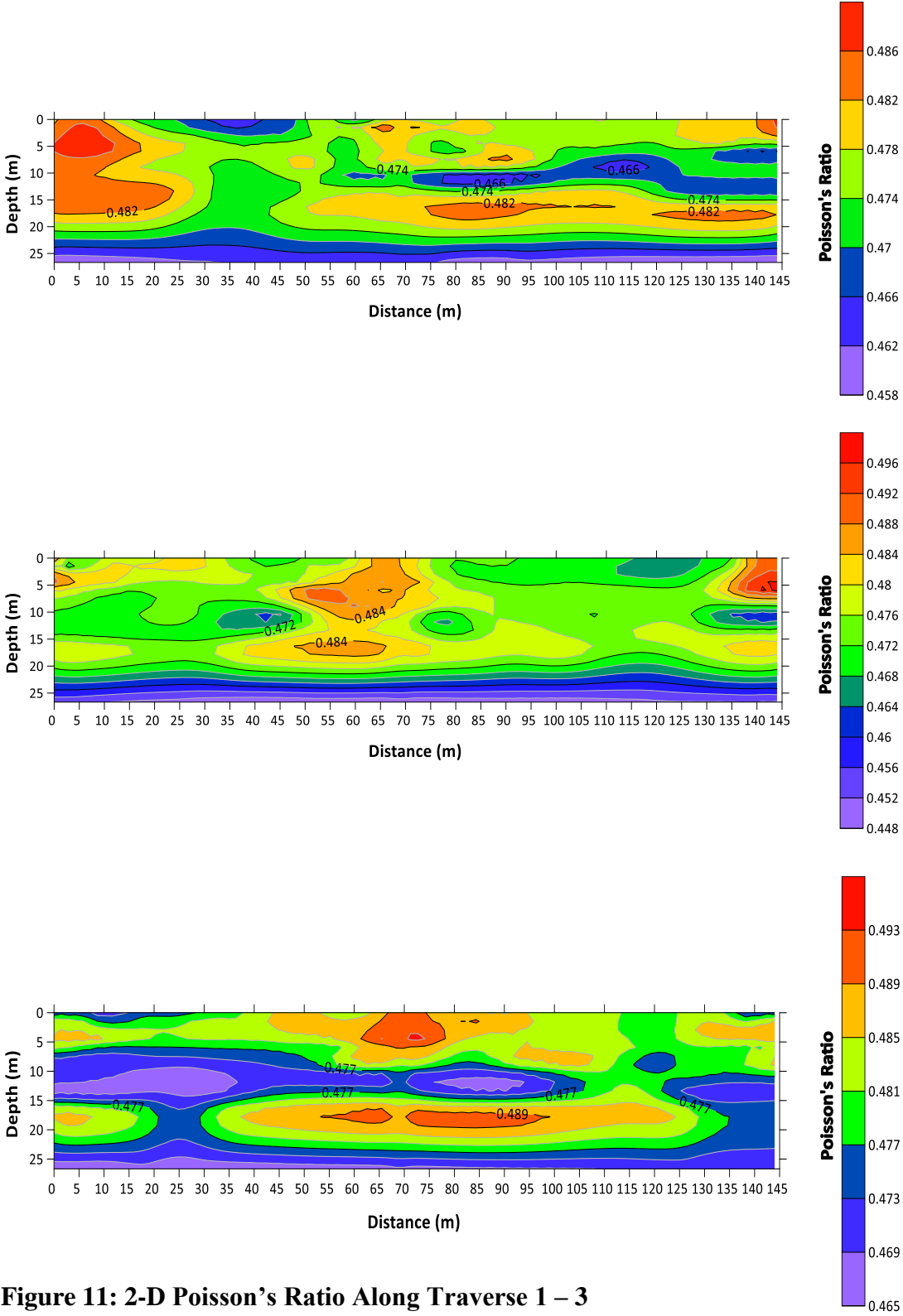


Figure 11: 2-D Poisson's Ratio Along Traverse 1 – 3

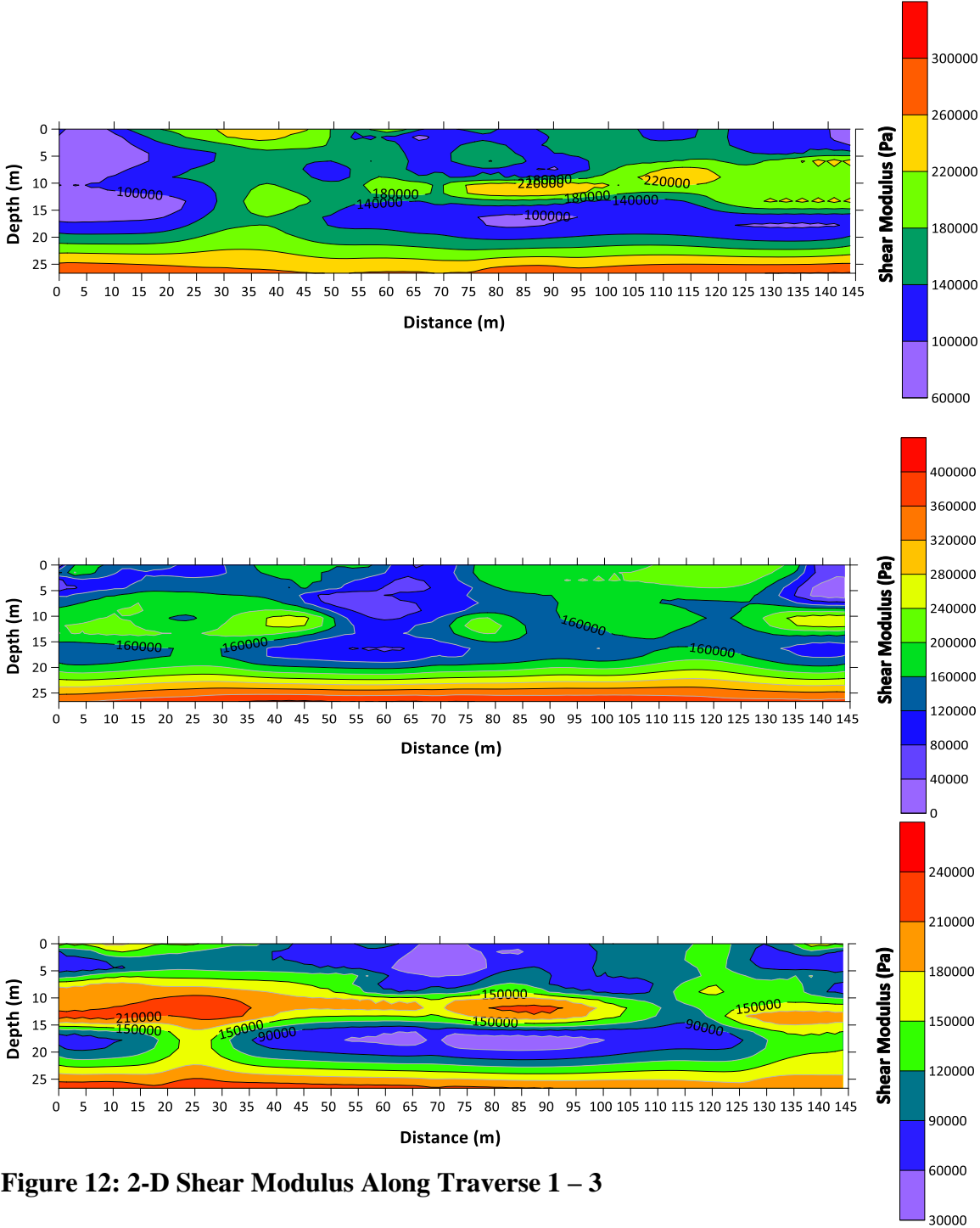


Figure 12: 2-D Shear Modulus Along Traverse 1 – 3

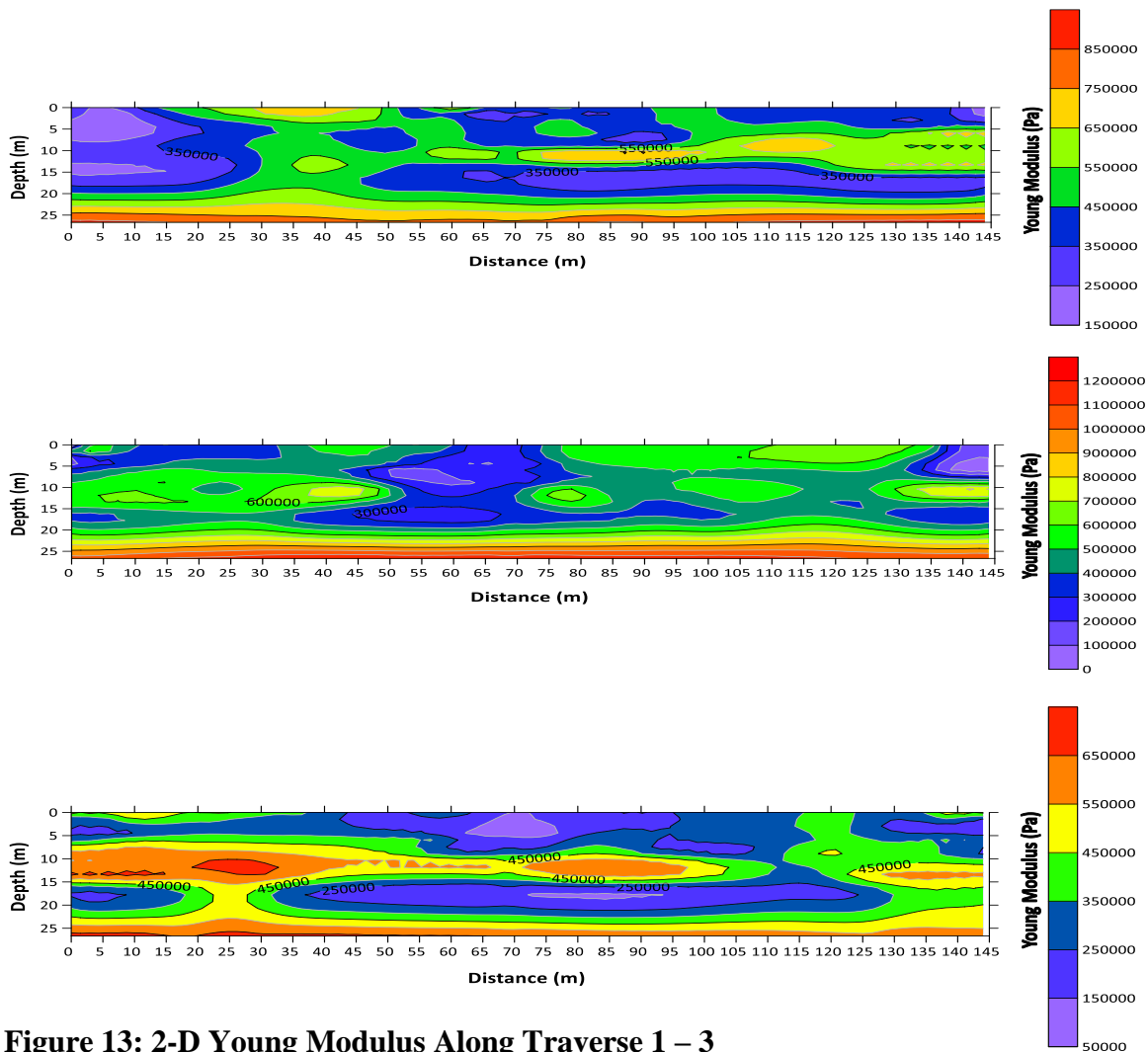


Figure 13: 2-D Young Modulus Along Traverse 1 – 3

Figure 8 showing the inverted shear wave velocity structures across traverse 1- 3 revealing to the distance and depth of 147 m and 37 m respectively with shear wave velocity ranging from 83 m/s to 465 m/s which implies soft to medium saturated clays/ dry sands and medium to stiff saturated clays/ dry sand/ wet sand sediments. Figure 9 displays the P-wave velocity structures across traverse 1 – 3 revealing to the distance and depth of 145 m and 27 m respectively. The P-wave velocity ranges from 1380 m/s to 1640 m/s depicting very soft saturated clays/ dry sands/ wet sands sediment and soft clay/ wet sands. Figure 10 revealing the Bulk Modulus structures across traverse 1 – 3 to the distance and depth 145 m and 27 m respectively. The Bulk Modulus ranges from 3.3 GPa to 5.9 GPa representative of very soft saturated clays/ dry sands/ wet sands sediment and soft clay/ wet sands. Figure 11 displays Poisson’s ratio structures along traverse 1 – 3 having Poisson’s ratio which ranges from 0.448 to 0.497 depicting very soft saturated clays/ dry sands/ wet sands sediment and soft clay/ wet sands. From Figure 12 representing the Shear Modulus structure with shear modulus ranging from 30 kPa to 440 kPa indicative of very soft saturated clays/ dry sands/ wet sands sediment and soft clay/ dry sands/ wet sands. Figure 13 is a representative of the Young’s Modulus structure revealing to the distance and depth of 145 m and

27 m respectively. The young's modulus ranges from 50 kPa to 1.3 GPa depicting very soft saturated clays/ dry sands/ wet sands sediment and soft clay/ wet sands sediments.

4.0. Conclusion

Joint investigation of gully erosion was carried using combined approach of Electrical Resistivity Tomography (ERT) and Multichannel Analysis of Surface Waves (MASW) in Iguosa. Acquired data from ERT and MASW were processed using Res2dinv and SeisImager2D refraction software respectively. The analysis and interpretation from 2-D geoelectric subsurface imaging reveals presence of topsoil, clay, sand and coarse sand. The shear wave velocity and elastic parameters reveals soil ranging from soft to medium-stiff and medium-stiff to stiff saturated soils. The erodibility of the study area has been identified.

Acknowledgement

I hereby acknowledge Mr. Toafik Adeleke and Adesegun Adefuwa for their availability and assistance during field data acquisition exercise for this study.

References

- [1] Chude, V.O., Ezendu C.O., Ugadu, M.E and Adiaha, M.S. (2021). A Review of the menace of soil erosion in Nigeria with specific reference to Southeastern States. *Nigeria Institute of Soil Science Colloquia SSSN* 44, 405-414
- [2] Mbaya, L.A. (2013). A Study of Inter-relations among Gully Variables in Gombe town, Gombe State, Nigeria. *Wudpecker J Geogr. Regional Plan.* 1(1):001-006.
- [3] Omran, Adel & Maerker, Michael & Hochschild, Volker. (2019). Assessment of Gully Erosion in Relation to Lithology in The Southwestern Zagros Mountains, Iran Using Aster Data, GIS and Stochastic Modeling. *Geografia Fisica e Dinamica Quaternaria.* 41. 95 104. 10.4461/GFDQ.2018.41.15.
- [4] Aigbadon, G.O., Ocheli, A. & Akudo, E.O (2021). Geotechnical evaluation of gully erosion and landslides materials and their impact in Iguosa and its environs, southern Nigeria. *Environ Syst Res* 10, 36 (2021). <https://doi.org/10.1186/s40068-021-00240-6>
- [5] Abdulfatai, I. A., Okunlola, I. A., Akande, W. G., Momoh, L. O., and Ibrahim, K. O. (2014). Review of Gully Erosion in Nigeria: Causes, Impacts and Possible Solutions. *Journal of Geosciences and Geomatics* Vol2(3): 125-129
- [6] Linus Unah (2020). Erosion crisis swallows homes and livelihoods in Nigeria. *Climate Home News*, Viewed 20 Aug. 2022, <https://www.climatechangenews.com/2020/01/20/erosion-crisis-swallows-homes-livelihoods-nigeria/>
- [7] Ezomo, F.O and Ifedili, S.O., (2005). Determination of water bearing formations at Osasogie Quarters by electrical Resistivity method. *Journal of civil and Environ. Systems Engr.* 6(1), 1-12.
- [8] Edward E. C., and Naven C., (2021). Use of Electrical Resistivity Tomography in investigating the internal structure of a landslide and its groundwater characterization (Nanka Landslide, Anambra State, Nigeria). *Journal of Applied Science and Engineering.* [doi.org/10.6180/jase.202208_25\(4\).0012](https://doi.org/10.6180/jase.202208_25(4).0012)
- [9] Uwaezuoke, C.C., K.S. Ishola and E. A. Ayolabi (2021). Electrical resistivity imaging and multichannel analysis of surface waves for mapping the subsurface of a Wetland Area of Lagos, Nigeria, NRIAG. *Journal of Astronomy and Geophysics*, 10:1, 300 319, DOI: 10.1080/20909977.2021.1927427
- [10] Hussain, Y., Hamza, O., Prado, R., Cárdenas-Soto, M., Borges, W., Dou, J., and Rodríguez R, J. (2020). Characterization of Sobradinho landslide in fluvial valley using MASW and ERT methods. *REM - International Engineering Journal.* 10.1590/0370-44672019730109.
- [11] Egwuonwu, G.N., Okoyeh, E.I. and Chikwelu E. E. (2019). 2DNear-Surface Litho-Structural Geophysical Investigation at the Vicinities of Two Gully-Erosion/Landslide Sites in South Eastern Nigeria. *IOSR Journal of Applied Geology and Geophysics (IOSR-JAGG)* 7.5 (2019): 70-75
- [12] Choon Park (2013). MASW for geotechnical site investigation. *The Leading Edge* 2013; 32 (6): 656-662. doi: <https://doi.org/10.1190/tle32060656.1>
- [13] Alile, O. M., Ujuanbi, O. and Evbuomwan, I. A. (2011). Geoelectric investigation of groundwater in Obaretin – Iyanomon locality, Edo state, Nigeria. *Journal of Geology and Mining Research*, 3(1), pp. 13 – 20.
- [14] Kearey, P. and Brooks, M. (1991). An introduction to geophysical exploration, 2nd Editions, Blackwell Scientific Publications, Oxford, 254-263pp.
- [15] Lowrie, W. (1997). *Fundamentals of Geophysics*. Cambridge University Press, New York, 354 pp.
- [16] Loke, M. H. (2000). Electrical imaging surveys for environmental and engineering studies: A practical guide to 2D and 3D surveys.
- [17] Loke, M. H. (1999). Time-lapse resistivity imaging inversion. Proceedings of the 5th Meeting of the Environmental and Engineering Geophysical Society European Section, Eml.
- [18] Telford, W. M., Telford, W. M., Geldart, L. P., Sheriff, R. E. and Sheriff, R. E. (1990). Applied geophysics. *Cambridge university press. Geomatics, Natural Hazards and Risk*, 10:1, 2291-2312, DOI:10.1080/19475705.2019.1685599
- [19] Park, Choon B, Richard Miller, Jianghai Xia, Nils Ryden, and Peter Ulriksen (2003). "The MASW Method - What and Where it is." EAGE 65th Conference and Exhibition. Stavanger.
- [20] Parasnis, D.S. (1997). Principles of Applied Geophysics. New York: Chapman & Hall.
- [21] Callister Jr., and William D. (2001). Fundamentals of Material Science and Engineering. New York: John Wiley and Sons, Inc.
- [22] Steeples, Don. (1998). "Near-Surface Seismology: A Short Course." Lawrence: Society of Exploration Geophysicist.
- [23] Khorshid Salman Zainal – Abdin (2016). Determination of Elastic Moduli and Geotechnical Parameters of the Upper Soil Layer Using Ultrasonic Waves in Al-Jadiriya Area – University of Baghdad-Iraq. *Iraqi Journal of Science*, Vol. 57(4c), pp. 2909 – 2921.